Inorg. Chem. **2007**, *46*, 939–948

Synthesis, Characterization, and Biomimetic Chemistry of *cis*-Oxosulfidomolybdenum(VI) Complexes Stabilized by an Intramolecular Mo(O)═S···S Interaction

Les J. Laughlin,[†] Aston A. Eagle,[†] Graham N. George,[‡] Edward R. T. Tiekink,[§] and Charles G. Young*,[†]

School of Chemistry, University of Melbourne, Victoria 3010, Australia, Stanford Synchrotron Radiation Laboratory, Stanford Linear Accelerator Center, Stanford University, P.O. Box 4349, MS 69, Stanford, California 94309, and Department of Chemistry, University of Texas at San Antonio, San Antonio, Texas 78249-0698

Received July 2, 2006

The reactions of jade-green $Tp^*Mo^{IV}O(S_2PR_2)$ [Tp* = hydrotris(3,5-dimethylpyrazol-1-yl)borate; R = Et, Pr^i, Ph] with propylene sulfide produce ochre-red $Tp^*Mo^{VI}OS\{SP(S)R_2\}$. The complexes have been characterized by microanalysis, mass spectrometry, cyclic voltammetry, spectroscopy (IR, NMR, UV–vis, and X-ray absorption), and X-ray crystallography. The distorted-octahedral isopropyl and phenyl derivatives feature a tridentate *fac*-Tp* ligand, a terminal oxo ligand, and a unique five-membered $Mo(═S)\{SP(═S)R_2$ ring moiety formed by a weak, intramolecular, bonding interaction between the Mo═S1 and (uncoordinated) S3═P moieties. The Mo═S1 [2.227(2) Å (R = Pr^i) and 2.200(2) Å (R = Ph)] and S1···S3 distances [2.396(3) Å (R = Pr^i) and 2.383(2) Å (R = Ph)] are indicative of a π-bonded Mo═S1 unit and a weak (bond order ca. $^1/_3$) S1···S3 interaction; the solid-state structures are maintained in solution according to S K-edge X-ray absorption data. The complexes react with excess cyanide to form thiocyanate and $Tp^*MoO(S_2PR_2)$, under anaerobic conditions, or $Tp^*MoO_2(S_2PR_2)$, under aerobic conditions; the latter models the production of thiocyanate and desulfo molybdenum hydroxylases upon cyanolysis of molybdenum hydroxylases. The complexes react with triphenylphosphine to give $Tp^*MoO(S_2PR_2)$ and $SPPh_3$, with cobaltocene or hydrosulfide ion to produce $[Tp^*Mo^VOS(S_2PR_2)]^-$, and with ferrocenium salts to yield $[Tp^*Mo^VO(S_3PR_2)]^+$; in the last two reactions, Mo(V) is produced by direct or induced internal redox reactions, respectively. The presence of the Mo(O)═S···S interaction does not radically lengthen the Mo═S bond in the complexes or preclude them from reactions typical of unperturbed oxosulfidomolybdenum(VI) complexes.

Introduction

Molybdenum hydroxylases are important in the metabolism of organic substrates such as purines, pyrimidines, and aldehydes.[1−5] Xanthine oxidase, the head of this large family of enzymes, is responsible inter alia for the catalytic conversion of hypoxanthine to xanthine and xanthine to uric acid during purine catabolism; the aldehyde oxidases, another important subclass of molybdenum hydroxylases, are involved in the production of retinoic acid and phytohormones and the metabolism of alcohol, drugs, and pollutants. These enzymes contain a mononuclear oxosulfidomolybdenum(VI)-oxidized active site, i.e., $(MPT)Mo^{VI}OS(OH_n)$ [MPT = *m*etal-binding *p*terin ene-1,2-di*t*hiolate (molybdopterin) ligand

* To whom correspondence should be addressed. E-mail: cgyoung@unimelb.edu.au.
[†] University of Melbourne.
[‡] Stanford University. Present address: Department of Geological Sciences, University of Saskatchewan, 114 Science Place, Saskatoon, Saskatchewan S7N 5E2, Canada.
[§] University of Texas at San Antonio.

(1) Hille, R. *Chem. Rev.* **1996**, *96*, 2757.
(2) Pilato, R. S.; Stiefel, E. I. In *Bioinorganic Catalysis*, 2nd ed.; Reedijk, J., Bouwman, E., Eds.; Marcel Dekker: New York, 1999; pp 81−152.
(3) Sigel, A., Sigel, H., Eds. *Metal Ions in Biological Systems*; Marcel Dekker: New York, 2002; Vol. 39.
(4) Tunney, J. M.; McMaster, J.; Garner, C. D. In *Comprehensive Coordination Chemistry II*; McCleverty, J. A., Meyer, T. J., Eds.; Elsevier Pergamon: Amsterdam, The Netherlands, 2004; Vol. 8, Chapter 8.18, pp 459−477.
(5) Young, C. G. In *Encyclopedia of Inorganic Chemistry 2*; King, R. B., Ed.; Wiley: Chichester, U.K., 2005; Vol. V, pp 3321−3340.

10.1021/ic061213d CCC: $37.00
Published on Web 01/11/2007

or nucleotide (R′) derivative].[1−5] There is strong evidence that the water-based ligand in xanthine oxidase is hydroxide (**I**),[6] and it is believed to be responsible for the hydroxylation of substrate during turnover.[1−5] The terminal sulfido ligand is also essential for catalysis (vide infra), but its precise roles remain uncertain. The carbon monoxide dehydrogenase from the aerobic eubacterium *Oligotropha carboxidovorans* is also classified as a molybdenum hydroxylase; it contains a unique (MPT)MoOX(μ-S)CuCys (X = OH[7] or O[8]) active site (**II**), and mechanisms involving the direct participation of the bridging sulfido ligand in the formation of thiocarbonate intermediates have been proposed.[7,9] In the absence of a direct mechanistic role,[9,10] the S atom is likely to be crucial to electron transfer/communication between the Mo and Cu centers during turnover.[11] Accordingly, there is a keen interest in understanding the fundamental chemistry of the terminal and bridging sulfido ligands in molybdenum hydroxylases and closely related model complexes.

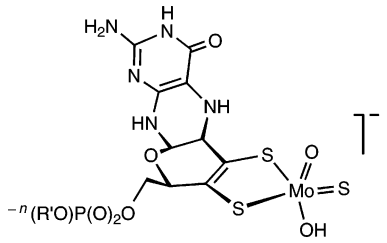

(**I**)

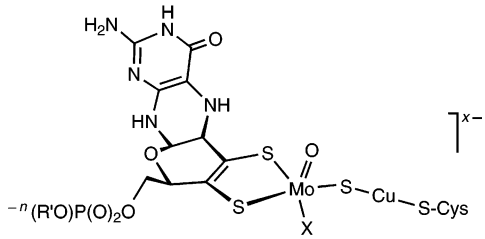

(**II**)

The deactivation of xanthine oxidase by cyanide, with concomitant formation of thiocyanate, and the reactivation of desulfo enzyme by sulfide provided the first indication of a catalytically essential, active-site S atom.[12,13] Prior to 1979, this cyanolyzable S was ascribed to persulfide,[13] cysteine,[14] or terminal sulfido[15] moieties on or near the Mo center. The detection of a short (2.15−2.25 Å) Mo−S interaction by extended X-ray absorption fine structure (EXAFS) spectroscopy provided direct evidence for the presence of a terminal sulfido ligand.[16] The same technique revealed that the oxidized desulfo enzymes contained a dioxomolybdenum(VI) center, permitting cyanolysis to be described in terms of eqs 1 and 2.[13,15c] Reactivation of desulfo enzyme by sulfide may be written as eq 3, although the mechanism of the reaction may involve a reduced intermediate.[15c] Indirect evidence for an oxosulfidomolybdenum(VI)-oxidized active site comes from the observation of very similar ^{33}S superhyperfine coupling in the electron paramagnetic resonance (EPR) spectra of reduced enzyme (the very rapid Mo(V) signal) and synthetic oxosulfidomolybdenum(V) complexes.[17] Carbon monoxide dehydrogenase is also deactivated by cyanide (through decupration and desulfurization) but can be reactivated by sequential provision of sulfide and Cu(I) under reducing conditions.[18]

$$[Mo^{VI}OS]^{2+}\ (\text{active}) + CN^- + H_2O \rightarrow [Mo^{IV}O(OH_2)]^{2+} + SCN^- \quad (1)$$

$$[Mo^{IV}O(OH_2)]^{2+} \rightarrow [Mo^{VI}O_2]^{2+}\ (\text{desulfo}) + 2H^+ + 2e^- \quad (2)$$

$$[Mo^{VI}O_2]^{2+} + SH^- \rightarrow [Mo^{VI}OS]^{2+} + OH^- \quad (3)$$

Mononuclear oxosulfidomolybdenum(VI) model complexes are poorly represented in the chemical literature.[19−22] Early examples include oxothiomolybdates, $[MoO_{4-n}S_n]^{2-}$,[23] hydroxylamido complexes, $MoOS(ONR_2)_2$,[24,25] and organometallic derivatives, $Cp^*MoOS(CH_2SiMe_3)$ ($Cp^* = \eta^5$-C_5Me_5).[26] These pseudotetrahedral complexes are prepared by sulfurization of dioxomolybdenum(VI) analogues, typically using hydrogen sulfide. More recently, $K_2[MoO_3S]$ was converted into $MoOS(OSiPh_3)_2L$ (L = phen or bpy derivative), following successive reactions with $ClSiPh_3/NEt_3$ and L.[27] Unfortunately, none of the above model complexes mimic the chemical behavior of the enzymes or are amenable

(6) Doonan, C. J.; Stockert, A.; Hille, R.; George, G. N. *J. Am. Chem. Soc.* **2005**, *127*, 4518.
(7) Dobbek, H.; Gremer, L.; Kiefersauer, R.; Huber, R.; Meyer, O. *Proc. Natl. Acad. Sci. U.S.A.* **2002**, *99*, 15971.
(8) Gnida, M.; Ferner, R.; Gremer, L.; Meyer, O.; Meyer-Klaucke, W. *Biochemistry* **2003**, *42*, 222.
(9) Siegbahn, P. E. M.; Shestakov, A. F. *J. Comput. Chem.* **2005**, *26*, 888.
(10) Hofmann, M.; Kassube, J. K.; Graf, T. *J. Biol. Inorg. Chem.* **2005**, *10*, 490.
(11) Gourlay, C.; Nielsen, D. J.; White, J. M.; Knottenbelt, S. Z.; Kirk, M. L.; Young, C. G. *J. Am. Chem. Soc.* **2006**, *128*, 2164.
(12) Szent-Gyorgi, A. *Biochem. Z.* **1926**, *173*, 275.
(13) Massey, V.; Edmondson, D. *J. Biol. Chem.* **1970**, *245*, 6595.
(14) Coughlan, M. P. *FEBS Lett.* **1977**, *81*, 1.
(15) (a) Williams, R. J. P.; Wentworth, R. A. D. *J. Less-Common Met.* **1974**, *36*, 405. (b) Gutteridge, S.; Tanner, S. J.; Bray, R. C. *Biochem. J.* **1978**, *175*, 887. (c) Wahl, R. C.; Rajagopalan, K. V. *J. Biol. Chem.* **1982**, *257*, 1354.
(16) (a) Bordas, J.; Bray, R. C.; Garner, C. D.; Gutteridge, S.; Hasnain, S. S. *Biochem. J.* **1980**, *191*, 499. (b) Cramer, S. P.; Wahl, R.; Rajagopalan, K. V. *J. Am. Chem. Soc.* **1981**, *103*, 7721. (c) Cramer, S. P.; Hille, R. *J. Am. Chem. Soc.* **1985**, *107*, 8164. (d) Turner, N. A.; Bray, R. C.; Diakun, G. P. *Biochem. J.* **1989**, *260*, 563.
(17) Wilson, G. L.; Greenwood, R. J.; Pilbrow, J. R.; Spence, J. T.; Wedd, A. G. *J. Am. Chem. Soc.* **1991**, *113*, 6803 and references cited therein.
(18) Resch, M.; Dobbek, H.; Meyer, O. *J. Biol. Inorg. Chem.* **2005**, *10*, 518.
(19) Young, C. G. *J. Biol. Inorg. Chem.* **1997**, *2*, 810.
(20) Young, C. G. In *Comprehensive Coordination Chemistry II*; McCleverty, J. A., Meyer, T. J., Eds.; Elsevier Pergamon: Amsterdam, The Netherlands, 2004; Vol. 4, Chapter 4.7, pp 415−527.
(21) Enemark, J. H.; Cooney, J. J. A.; Wang, J.-J.; Holm, R. H. *Chem. Rev.* **2004**, *104*, 1175.
(22) McMaster, J.; Tunney, J. M.; Garner, C. D. *Prog. Inorg. Chem.* **2004**, *52*, 539.
(23) Müller, A.; Diemann, E.; Jostes, R.; Bögge, H. *Angew. Chem., Int. Ed. Engl.* **1981**, *20*, 934.
(24) Wieghardt, K.; Hahn, M.; Weiss, J.; Swiridoff, W. *Z. Anorg. Allg. Chem.* **1982**, *492*, 164.
(25) Bristow, S.; Collison, D.; Garner, C. D.; Clegg, W. *J. Chem. Soc., Dalton Trans.* **1983**, 2495.
(26) Faller, J. W.; Ma, Y. *Organometallics* **1989**, *8*, 609.
(27) Thapper, A.; Donahue, J. P.; Musgrave, K. B.; Willer, M. W.; Nordlander, E.; Hedman, B.; Hodgson, K. O.; Holm, R. H. *Inorg. Chem.* **1999**, *38*, 4104.

to clean reductions.[19] We have exploited O atom transfer (OAT, eq 4) and S atom transfer (SAT, eq 5) reactions in the preparation of mononuclear oxosulfidomolydenum(VI) complexes such as Tp*MoOS{SP(S)Pr$^i_2$} [Tp* = hydrotris-(3,5-dimethylpyrazol-1-yl)borate],[28] Tp′MoOS{SP(S)R$_2$} [Tp′ = hydrobis(3-isopropylpyrazolyl-1-yl)(5-isopropylpyrazolyl-1-yl)borate; R = Pr^i, Ph],[29] and Tp^{iPr}MoOS(OAr) [Tp^{iPr} = hydrotris(3-isopropylpyrazol-1-yl)borate; OAr = phenolate].[30] Mononuclear oxosulfido(dithiolene)molybdenum complexes are currently unknown.[21]

$$[Mo^{IV}S]^{2+} + [O] \rightarrow [Mo^{VI}OS]^{2+} \quad (4)$$

$$[Mo^{IV}O]^{2+} + [S] \rightarrow [Mo^{VI}OS]^{2+} \quad (5)$$

Here, we provide a full account of our studies of *cis*-oxosulfidomolybdenum(VI) complexes stabilized by a weak, intramolecular Mo(O)═S···S interaction, viz., Tp*MoOS{SP(S)Pr$^i_2$} (hereafter, the S···S interaction will not be explicitly drawn). A number of communications have reported leading results; these include the synthesis and crystal structure of Tp*MoOS(S$_2$PPr$^i_2$),[28] mention of its reaction with cyanide,[28] and aspects of its redox chemistry [as compared and contrasted with the redox behavior of a (dithio)oxomolybdenum(IV) "redox tautomer"].[31] The anionic complex, [Tp*MoOS(S$_2$PPr$^i_2$)]$^-$, has been reported in connection with the reactivity of dioxomolybdenum(VI) (n = 2) and oxomolybdenum(IV) (n = 1) species, Tp*MoO$_n$(S$_2$PR$_2$).[32] In this paper, we report complete details of the synthesis, characterization, crystal structures, and reactivity of the title complexes; unreported results include the crystal structure of Tp*MoOS(S$_2$PPh$_2$), Mo K-edge EXAFS spectroscopy, S K-edge X-ray absorption spectroscopy (XAS), electrochemical data, and details of reactions leading to biologically relevant Mo(V) species or biomimetic outcomes, e.g., a model for the cyanolysis of molybdenum hydroxylases. Scheme 1 summarizes the chemistry described herein.

Scheme 1

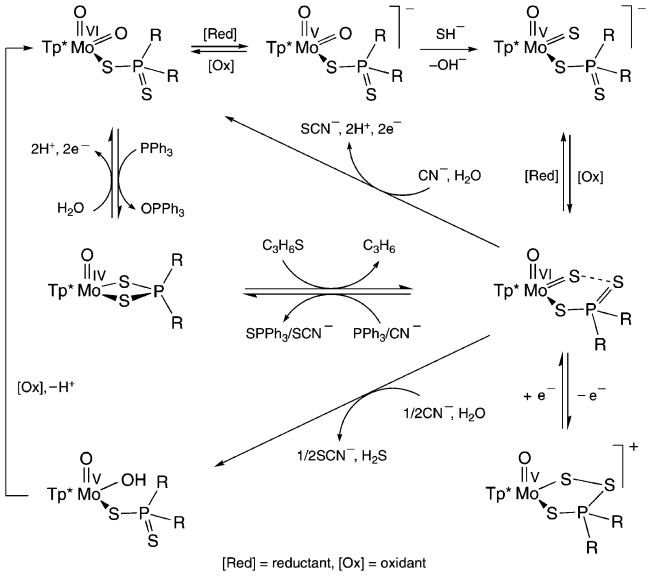

Experimental Section

Materials and General Methods. All reactions were performed under an atmosphere of N_2 using standard Schlenk techniques and dried, deoxygenated solvents. The tetrahydrofuran (THF) and acetonitrile employed in EPR experiments were rigorously dried by reflux over and distillation from activated alumina under N_2. The compounds Tp*MoO(S$_2$PR$_2$),[32] Tp*MoSCl$_2$,[33] [FeCp$_2$]PF$_6$ (Cp = η^5-C$_5$H$_5$),[34] and NEt$_4$[CN][35] were prepared by literature methods. Cobaltocene, CoCp$_2$, was obtained from the Aldrich Chemical Co. and sublimed prior to use. O_2 gas was dried by slow passage through a 4-Å molecular sieve. All other reagents were analytical reagent grade or better. Chromatography was performed on a 50-cm column (2-cm diameter) using Merck Art. 7734 Keiselgel 60. IR spectra were recorded on a Perkin-Elmer 1430 spectrophotometer as pressed KBr discs. ^{1}H and ^{31}P{^{1}H} NMR were obtained using a Varian Fourier transform (FT) Unity-300 spectrometer and were referenced to internal CHCl$_3$ (δ 7.23) and external 85% H$_3$PO$_4$ (δ 0), respectively. EPR spectra were recorded on a Bruker FT ECS-106 spectrometer using 1,1-diphenyl-2-picrylhydrazyl as the reference. Electronic spectra were obtained on Shimadzu UV-240 and Hitachi 150-20 UV spectrophotometers using matched quartz cells. Electrochemical experiments were performed using an Autolab PG-STAT30 instrument with a 2-mm glassy carbon working electrode, a platinum auxiliary electrode, and an Ag/AgNO$_3$ (0.01 M in MeCN) electrode incorporated into a salt bridge containing supporting electrolyte to minimize Ag$^+$ leakage. Solutions of the complexes (1−2 mM) in 0.1 M NBu$^n_4$BF$_4$/acetonitrile were employed, and potentials were referenced to internal ferrocene ($E_{1/2}$ = +0.40 V vs SCE).[36] Potentials are reported relative to the saturated calomel electrode (SCE). Mass spectra were recorded on a Vacuum Generators VG ZAB 2HF mass spectrometer. Microanalyses were performed by Atlantic Microlabs, Norcross, GA.

Syntheses. Tp*MoOS(S$_2$PEt$_2$). A green solution of Tp*MoO(S$_2$PEt$_2$) (0.15 g, 0.267 mmol) and propylene sulfide (0.22 mL, 2.7 mmol) in 1,2-dichloroethane (20 mL) was refluxed for 1 day. The deep-red solution was reduced to a minimum volume and column-chromatographed on silica gel, using dichloromethane as the eluent. The main red band was collected, and the compound was recrystallized from dichloromethane/methanol. The yield of ochre-red crystals was 0.13 g, 82%. Anaerobic decomposition of the compound over a period of days prevented the collection of microanalytical data. IR (KBr): ν(BH) 2550 m, ν(CN) 1540 s, ν(Mo═O) 930, ν(MoS) 465 cm^{-1}. ^{1}H NMR (CDCl$_3$): δ 1.09 and 1.50 (each dt, 3H, ^3J = 7 Hz, J_{PH} = 20 Hz, 2CH$_2$CH_3), 2.12, 2.23, 2.39, 2.40, 2.70, 2.76 (each s, 3H, 6CH_3 of Tp*), 2.0−3.0 (obscured m, 4H, 2CH_2), 5.52, 5.82, 5.91 (each s, 1H, 3CH of Tp*).

Tp*MoOS(S$_2$PPr$^i_2$). Prepared according to the literature method.[28] Additional characterization data include the following. IR (KBr): ν(BH) 2550 m, ν(CN) 1540 s, ν(Mo═O) 930, ν(MoS) 465 cm^{-1}.

(28) Eagle, A. A.; Laughlin, L. J.; Young, C. G.; Tiekink, E. R. T. *J. Am. Chem. Soc.* **1992**, *114*, 9195.
(29) Young, C. G.; Laughlin, L. J.; Colmanet, S.; Scrofani, S. D. B. *Inorg. Chem.* **1996**, *35*, 5368.
(30) Doonan, C. J.; Nielsen, D. J.; Smith, P. D.; White, J. W.; George, G. N.; Young, C. G. *J. Am. Chem. Soc.* **2006**, *128*, 305.
(31) Hill, J. P.; Laughlin, L. J.; Gable, R. W.; Young, C. G. *Inorg. Chem.* **1996**, *35*, 3447.
(32) Laughlin, L. J.; Young, C. G. *Inorg. Chem.* **1996**, *35*, 1050.
(33) Young, C. G.; Enemark, J. H.; Collison, D.; Mabbs, F. E. *Inorg. Chem.* **1987**, *26*, 2925.
(34) Desbois, M.-H.; Astruc, D. *New J. Chem.* **1989**, *13*, 595.
(35) Traill, P. R.; Tiekink, E. R. T.; O'Connor, M. J.; Snow, M. R.; Wedd, A. G. *Aust. J. Chem.* **1986**, *39*, 1287.
(36) Connelly, N. G.; Gieger, W. E. *Chem. Rev.* **1996**, *96*, 877.

$^{31}P\{^1H\}$ NMR ($CDCl_3$): δ 108 ($W_{1/2}$ = 15 Hz). Electrochemistry (MeCN): E_{pc} = −0.67 V (irreversible reduction), E_{pa} = −0.30, +0.12, and +0.49 V (irreversible), $E_{1/2}$ = +0.66 V (ΔE_{pp} = 59 mV, I_{pa}/I_{pc} = 0.92, reversible oxidation).

Tp*MoOS(S_2PPh_2). A green solution of Tp*MoO(S_2PPh_2) (1.0 g, 1.52 mmol) and propylene sulfide (1.2 mL, 15.2 mmol) in 1,2-dichloroethane (20 mL) was stirred at 60 °C in a sealed flask under a slight vacuum for 1 day. The deep-red solution was reduced to minimal volume and column-chromatographed on silica gel, using dichloromethane/pentane (3:1) as the eluent. The main red fraction was collected, and the compound was recrystallized from dichloromethane/methanol (with prolonged cooling). The yield of red needles was 0.84 g, 80%.

Anal. Calcd for $C_{27}H_{32}BMoN_6OPS_3$: C, 46.96; H, 4.67; N, 12.17; S, 13.93. Found: C, 47.03; H, 4.68; N, 12.16; S, 13.96. MS: *m*/*z* 692 (10%, $[M]^+$), 660 (8%, $[M - S]^+$), 628 (6%, $[M - 2S]^+$), 445 (5%, $[M - S_2PPh_2]^+$). IR (KBr): ν(BH) 2550 m, ν(CN) 1540 s, ν(Mo=O) 930, ν(MoS) 490 cm^{-1}. ^1H NMR ($CDCl_3$): δ 2.18, 2.25, 2.40, 2.40, 2.68, 2.71 (each s, 3H, 6C*H*$_3$ of Tp*), 5.55, 5.91, 5.93 (each s, 1H, 6C*H* of Tp*), 7.4−8.1 (m, 10H, 2Ph). $^{31}P\{^1H\}$ NMR ($CDCl_3$): δ 77 ($W_{1/2}$ = 20 Hz). Electronic spectrum (CH_2Cl_2): 455 (2890), 345 nm (ϵ 4430 M^{-1} cm^{-1}). Electrochemistry (MeCN): E_{pc} = −0.55 V (irreversible reduction), E_{pa} = +0.06, +0.13, and +0.48 V (irreversible), $E_{1/2}$ = +0.66 V (ΔE_{pp} = 59 mV, I_{pa}/I_{pc} = 0.95, reversible oxidation).

Tp*MoSCl($S_2PPr^i_2$). A solution of $HS_2PPr^i_2$ (0.863 mL, 5.04 mmol) and triethylamine (0.703 mL, 5.04 mmol) in dichloromethane (20 mL) was added to a stirred solution of Tp*MoSCl$_2$ (1.137 g, 2.29 mmol) in dichloromethane (35 mL). The resulting mixture was stirred for 1 day, reduced to dryness, and then chromatographed on silica using dichloromethane as the eluent. The major orange band was collected, evaporated to dryness, and recrystallized from dichloromethane/methanol. The yield of orange-red crystals was 1.30 g, 90%. In air, solutions of the compound decomposed to produce Tp*MoOS($S_2PPr^i_2$), with properties identical with those of an authentic sample.[28]

Anal. Calcd for $C_{21}H_{36}BClMoN_6PS_3$: C, 39.29; H, 5.65; N, 13.09; S, 14.99; Cl, 5.52. Found: C, 39.01; H, 5.60; N, 12.97; S, 14.87; Cl, 5.73. MS: *m*/*z* 643 (25%, $[M]^+$). IR (KBr): ν(BH) 2550 m, ν(CN) 1530 s, ν(PS) 645 m, ν(Mo=S) 500 m, ν(MoCl) 300 s cm^{-1}. Electronic spectrum (CH_2Cl_2): 390 nm (ϵ 8900 M^{-1} cm^{-1}). EPR (THF): g = 1.940, $a(^{95,97}Mo)$ = 45.3 × 10^{-4} cm^{-1}. Electrochemistry (MeCN): E_{pc} = −1.14 V (irreversible reduction), E_{pa} = −0.59 V (irreversible), $E_{1/2}$ = +0.65 V (ΔE_{pp} = 68 mV, I_{pa}/I_{pc} = 1.05, reversible oxidation).

Kinetics Studies. Reactions were followed spectrophotometrically using a Shimadzu UV-240 spectrophotometer and matched quartz cells. Solutions were equilibrated at the specified temperatures prior to use. Pseudo-first-order conditions were employed for each run with [C_3H_6S]/[Mo complex] ratios over the range from 400:1 to 50:1 and at temperatures of 35, 45, and 55 °C. The initial concentration of the Mo complex was 6.0 mM. Fresh solutions were prepared on a daily basis.

Crystallography. Crystals of a disordered polymorph of Tp*MoOS($S_2PPr^i_2$) were grown by slow diffusion of methanol into dichloromethane solutions of the compound. However, ordered, diffraction-quality crystals (as well as the disordered polymorph) were only obtained by slow diffusion of methanol into a dichloromethane solution of Tp*MoSCl($S_2PPr^i_2$) in air. Crystals of Tp*MoOS(S_2PPh_2) were grown by slow diffusion of methanol into dichloromethane solutions of the compound.

Intensity data for a crystal 0.02 × 0.11 × 0.24 mm^3 (0.03 × 0.16 × 0.39 mm^3 for R = Ph) were measured at 293 °C on an Enraf-Nonius CAD4F (Rigaku AFC6R for R = Ph) diffractometer fitted with graphite-monochromatized Mo Kα radiation, λ = 0.710 73 Å. The $\omega-2\theta$ scan technique was employed to measure data up to a maximum Bragg angle of 22.5° (27.8° for R = Ph). Each data set was corrected for Lorentz and polarization effects, and an analytical (R = Pr^i)[37] or empirical (R = Ph)[38] absorption correction was applied. Relevant crystal data are given in Table 1.

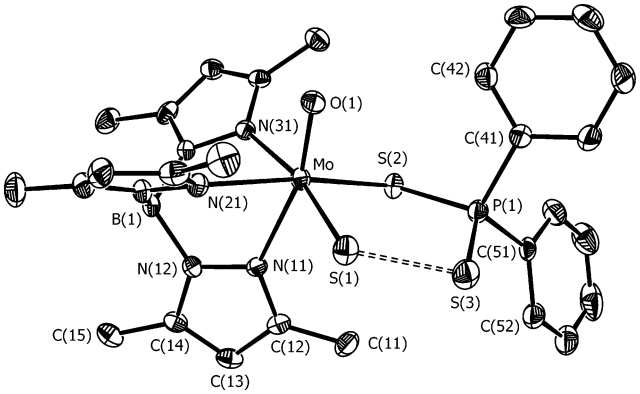

Figure 1. Molecular structure of Tp*MoOS(S_2PPh_2). The numbering schemes for the atoms in the rings containing N21 and N31 are the same as that shown for the ring containing N11.

Table 1. Crystallographic Data

	Tp*MoOS($S_2PPr^i_2$)	Tp*MoOS(S_2PPh_2)
formula	$C_{21}H_{36}BMoN_6OPS_3$	$C_{27}H_{32}BMoN_6OPS_3$
fw	622.48	690.51
space group	$P2_1/n$	$P2_1/n$
a, Å	12.601(1)	10.153(4)
b, Å	10.899(1)	20.993(3)
c, Å	20.595(3)	13.985(2)
β, deg	90.09(1)	91.81(2)
V, $Å^3$	2828.5	2979(1)
Z	4	4
ρ, g cm^{-3}	1.462	1.539
R	0.041	0.044
R_w	0.041	0.039

The structures were solved by Patterson (R = Pr^i) or direct methods (R = Ph) and refined by a full-matrix least-squares procedure based on *F*.[37,39] Non-H atoms were refined with anisotropic displacement parameters, and H atoms were included in the model at their calculated positions. Each refinement was continued until convergence, employing a weighting scheme of the form $k/[\sigma^2(F) + |g|F^2]$. The analysis of variance showed no special features, indicating that an appropriate weighting scheme had been applied. Final refinement details are collected in Table 1, and the numbering schemes employed are displayed in Figure 1, drawn using ORTEP[40] at the 35% probability level. Selected distances and angles are presented in Table 2.

XAS. Data Collection. XAS was carried out at the Stanford Synchrotron Radiation Laboratory with the SPEAR storage ring containing 55−90 mA at 3.0 GeV. Mo K-edge XAS spectra were collected on beamline 7-3 using a Si(220) double-crystal monochromator with an upstream vertical aperture of 1 mm and a wiggler field of 1.8 T. Harmonic rejection was accomplished by detuning one monochromator crystal to approximately 60% off-peak. An

(37) Sheldrick, G. M. *SHELX-76, Program for Crystal Structure Determination*; University of Cambridge: Cambridge, U.K., 1976.
(38) Sheldrick, G. M. *Acta Crystallogr.* **1990**, *A46*, 467.
(39) *teXsan: Structure Analysis Software*; Molecular Structure Corp.: The Woodlands, TX, 1997.
(40) Johnson, C. K. *ORTEP-II, Report ORNL-5138*; Oak Ridge National Laboratory: Oak Ridge, TN, 1976.

Table 2. Selected Bond Distances (Å) and Angles (deg)

atoms	Tp*MoOS($S_2PPr^i_2$)	Tp*MoOS(S_2PPh_2)
Mo−O1	1.702(4)	1.662(3)
Mo−S1	2.227(2)	2.200(2)
Mo−S2	2.431(2)	2.389(2)
Mo−N11	2.388(5)	2.347(4)
Mo−N21	2.204(5)	2.194(4)
Mo−N31	2.280(6)	2.237(4)
S1···S3	2.396(3)	2.383(2)
S2−P1	2.052(2)	2.035(2)
S3−P1	2.007(3)	1.980(2)
O1−Mo−S1	102.4(2)	102.9(1)
O1−Mo−S2	100.9(1)	100.4(1)
O1−Mo−N11	161.8(2)	163.5(2)
O1−Mo−N21	92.0(2)	90.7(2)
O1−Mo−N31	86.2(2)	88.3(2)
S1−Mo−S2	92.5(1)	92.90(5)
S1−Mo−N11	93.5(1)	91.2(1)
S1−Mo−N21	91.8(1)	92.2(1)
S1−Mo−N31	170.6(1)	167.8(1)
S2−Mo−N11	87.1(1)	87.2(1)
S2−Mo−N21	165.3(1)	166.5(1)
S2−Mo−N31	89.3(1)	89.9(1)
N11−Mo−N21	78.6(2)	80.2(1)
N11−Mo−N31	77.4(2)	77.0(1)
N21−Mo−N31	84.3(2)	82.7(1)
Mo−S1−S3	115.5(1)	115.36(7)
S1−S3−P1	98.1(1)	98.65(9)
S2−P1−S3	113.7(1)	114.81(9)
Mo−S2−P1	108.9(1)	109.76(7)

Oxford Instruments CF1208 continuous-flow liquid-He cryostat maintained a constant sample temperature of 10 K. Mo K-edge XAS spectra were measured in transmittance mode using Ar-filled ionization chambers. A spectrum of Mo foil was collected simultaneously with that of the sample, and spectra were calibrated with reference to the lowest energy inflection point of the K-edge, assigned as 20 003.9 eV. Solid samples were diluted by grinding with boron nitride so that the maximum absorbance was approximately 2.0. Solutions were prepared in chloroform (ca. 100 mM), then frozen, and examined at 10 K.

S K-edge spectra were performed on beamline 6-2 using a Si(111) double-crystal monochromator and a wiggler field of 1.0 T. Harmonic rejection was accomplished by using a flat Ni-coated mirror downstream of the monochromator adjusted so as to have a cutoff energy of about 4500 eV. The incident intensity was monitored using an ion chamber contained in a (flowing) He-filled flight path. Energy resolution was optimized by decreasing the vertical aperture upstream of the monochromator and quantitatively determined to be 0.51 eV by measuring the width of the 2471.4-eV 1s → $\pi^*(3b_1)$ transition of gaseous SO_2, which corresponds to a transition to a single orbital rather than to a band of orbitals, which can be the case with solid standards.[41] XAS was monitored by recording the total electron yield, and the energy scale was calibrated with reference to the lowest energy peak of the sodium thiosulfate standard ($Na_2S_2O_3{\cdot}5H_2O$), which was assumed to be 2469.2 eV.[42] Solutions were prepared in chloroform (ca. 100 mM) and examined at ambient temperature.

Data Analysis. Data were analyzed using the EXAFSPAK suite of computer programs (http://ssrl.slac.stanford.edu/EXAFSPAK.html), and no smoothing or related operations were performed upon the data. The EXAFS oscillations $\chi(k)$ were quantitatively analyzed by curve fitting using ab initio theoretical phase and amplitude functions calculated using the program FEFF (version 8.2) of Rehr and co-workers.[43,44] The small outer-shell EXAFS of complexes containing Tp* was modeled using the multiple-scattering capabilities of *feff* and an idealized facially tridentate ligand structure. Peak positions in near-edge spectra were estimated by curve fitting to a sum of pseudo-Voigt peaks using the program EDG_FIT (pseudo-Voigt deconvolution).[45]

Results

Synthesis and Kinetics. The reaction of jade-green Tp*MoO(S_2PR_2) with excess propylene sulfide in chlorinated solvents produced ochre-red Tp*MoOS(S_2PR_2), according to eq 6. These SAT reactions parallel well-known OAT processes[46,47] and involve a formal two-electron oxidation of Mo(IV) to Mo(VI).

$$\text{Tp*MoO}(S_2PR_2) + C_3H_6S \rightarrow \text{Tp*MoOS}(S_2PR_2) + C_3H_6 \quad (6)$$

The reactions were slow at room temperature (7 days), and elemental S failed to produce a similar transformation. The products were isolated by column chromatography and recrystallized to remove residual propylene sulfide and a trace of EPR-active byproduct. The dimethyl- and diethyldithiophosphinate analogues were unstable and could not be completely characterized. The related dithiophosphate complexes Tp*MoOS{$S_2P(OR)_2$} (R = Me, Et, Pr^i) were generated in situ but were unstable with respect to $[\text{Tp*Mo}^{V}\text{O}]_2(\mu\text{-O})(\mu\text{-}S_2)$.[48] Consequently, we restrict further discussion to stable derivatives, Tp*MoOS(S_2PR_2) (R = Pr^i, Ph). These oxygen- and water-stable complexes are soluble in chlorinated solvents, partially soluble in polar solvents such as acetonitrile, and insoluble in alcohols and hydrocarbons.

The kinetics of the reaction in eq 6 (R = Pr^i) were investigated in 1,2-dichloroethane solution under pseudo-first-order conditions.[49] Disappearance of the 677-nm band of Tp*MoO($S_2PPr^i_2$) was used to monitor each reaction, and tight isosbestic points were obtained in all cases. The reactions were first-order with respect to Tp*MoO($S_2PPr^i_2$), and plots of $\ln(A_t/A_0)$ vs time were linear to at least 90% reaction completion. The reactions were also first-order in propylene sulfide as shown by linear plots of k_{obs} vs $[C_3H_6S]_0$, leading to an overall second-order rate law, eq 7. Second-order rate constants, k, were determined at three temperatures, viz., $7.0(1) \times 10^{-6}$ M^{-1} s^{-1} at 35 °C, $1.6(1) \times 10^{-5}$ M^{-1} s^{-1} at 45 °C, and $3.2(1) \times 10^{-5}$ M^{-1} s^{-1} at 55 °C. Plots of ln k

(41) Song, I.; Rickett, B.; Janavicius, P.; Payer, J. H.; Antonio, M. R. *Nucl. Instrum. Methods Phys. Res., Sect. A* **1995**, *360*, 634.
(42) Sekiyama, H.; Kosugi, N.; Kuroda, H.; Ohta, T. *Bull. Chem. Soc. Jpn.* **1986**, *59*, 575.
(43) Rehr, J. J.; Mustre de Leon, J.; Zabinsky, S. I.; Albers, R. C. *J. Am. Chem. Soc.* **1991**, *113*, 5135.
(44) Mustre de Leon, J.; Rehr, J. J.; Zabinsky, S. I.; Albers, R. C. *Phys. Rev.* **1991**, *B44*, 4146.
(45) Pickering, I.; George, G. N. *Inorg. Chem.* **1995**, *34*, 3142.
(46) (a) Holm, R. H. *Chem. Rev.* **1987**, 1401. (b) Holm, R. H. *Coord. Chem. Rev.* **1990**, *100*, 183.
(47) Young, C. G. In *Biomimetic Oxidations Catalyzed by Transition Metal Complexes*; Meunier, B., Ed.; Imperial College Press: London, 2000; pp 415−459.
(48) (a) Roberts, S. A.; Young, C. G.; Cleland, W. E., Jr.; Yamanouchi, K.; Ortega, R. B.; Enemark, J. H. *Inorg. Chem.* **1988**, *27*, 2647. (b) Xiao, Z.; Enemark, J. H.; Wedd, A. G.; Young, C. G. *Inorg. Chem.* **1994**, *33*, 3438.
(49) Wilkins, R. G. *Kinetics and Mechanisms of Reactions of Transition Metal Complexes*, 2nd ed.; VCH: New York, 1991.

vs T^{-1} permitted the calculation of the following thermodynamic parameters: $\Delta H^{\ddagger} = 61(1)$ kJ mol^{-1}, $\Delta S^{\ddagger} = -142(2)$ J K^{-1} mol^{-1}, and $\Delta G^{\ddagger} = 105(2)$ kJ mol^{-1} at 35 °C.

$$-\mathrm{d}[\mathrm{Tp^*MoO(S_2PPr^i_2)}]/\mathrm{dt} = k[\mathrm{Tp^*MoO(S_2PPr^i_2)}][\mathrm{C_3H_6S}] \quad (7)$$

An associative mechanism for SAT from propylene sulfide to Tp*MoO(S_2PR_2) complexes is consistent with the second-order rate law (eq 7) and the large negative $\Delta S^{\ddagger}$ values. It is probable that cleavage of a Mo−S bond is initiated by close approach and binding of the substrate, followed by SAT to form Tp*MoOS(S_2PR_2) and propene. Similar kinetics characterize OAT reactions involving Tp*MoO(S_2PR_2) and Me_2SO or pyridine *N*-oxide, but the reactions are faster [k ranges from 9.0(1) × 10^{-5} to 1.54(5) × 10^{-3} M^{-1} s^{-1} at 40 °C].[32] The main reason for this difference lies in the values of $\Delta S^{\ddagger}$ for the two processes. Analogous oxosulfidomolybdenum(VI) complexes of Tp′ may be prepared by SAT to Tp′MoO(S_2PR_2) or OAT to Tp′MoS(S_2PR_2).[29]

Characterization Data. The compounds were characterized by analytical, mass spectrometric, spectroscopic, and X-ray crystallographic techniques. IR spectra exhibited a strong ν(Mo═O) band at 930 cm^{-1}, ca. 30 cm^{-1} lower in energy than the corresponding band for Tp*MoO(S_2PR_2),[32] Tp*MoO(pyS_2) (pyS_2 = pyridine-2-dithio),[31] and related oxomolybdenum(IV) complexes[20] but higher in energy than the corresponding vibrational mode in unperturbed oxosulfidomolybdenum(VI) complexes, such as MoOS(ONR_2)$_2$ (913−908 cm^{-1}),[24] MoOS($OSiPh_3$)$_2$L (L = bpy or phen derivative; 920−895 cm^{-1}),[27] and Tp$^{i\mathrm{Pr}}$MoOS(OAr) (915−902 cm^{-1}).[30] This indicates a weakening of the Mo═O bond by the competing π-bonded sulfido ligand, albeit to a lesser extent than was observed in unperturbed oxosulfidomolybdenum(VI) complexes. Only a weak band was observed in the region typical of the ν(Mo═S) mode in unperturbed oxosulfidomolybdenum(VI) complexes (520−460 cm^{-1}),[20] but this could not confidently be assigned to the ν(Mo═S) mode; Tp* ligand bands are also observed in this region.[32] Other bands characteristic of the Tp* and $S_2PR_2^-$ ligands were also observed. The high energy of the ν(P═S) stretch for both complexes is indicative of strong P−S bonding.

^{1}H NMR spectra exhibited five singlet methyl resonances (3:3:6:3:3 integrated ratio) and three singlet methine resonances (1:1:1 integrated ratio), assignable to the Tp* ligand in molecules of C_1 symmetry. In the spectrum of Tp*MoOS($S_2PPr^i_2$), four overlapping doublet-of-doublet resonances at δ 1.22−1.60 were observed for the diastereotopic isopropyl methyl groups. These resonances collapsed to four doublet resonances upon ^{31}P decoupling. Resonances due to the phenyl protons of Tp*MoOS(S_2PPh_2) were observed in the δ 7.4−8.1 region. The ^{31}P{^{1}H} NMR spectra of Tp*MoOS($S_2PPr^i_2$) and Tp*MoOS(S_2PPh_2) exhibited narrow resonances at δ 108 and δ 77, respectively. The resonances are deshielded by 12−28 ppm relative to the dioxo analogues, consistent with the involvement of the P═S unit in a dative Mo═S···S interaction. The resonances of the dioxo- and oxosulfidomolybdenum(VI) complexes are shielded by well over 50 ppm relative to complexes such as Tp*MoO(S_2PR_2) and Tp′MoE(S_2PPh_2) (E = O, S), bearing bidentate dithiophosphinate ligands.[29,32]

The deep-red color and electronic spectra of the complexes are typical of oxosulfidomolybdenum(VI) complexes, e.g., MoOS(ONR_2)$_2$ (λ 413 nm, ϵ 500 M^{-1} cm^{-1}),[24,25] MoOS($OSiPh_3$)$_2$(bpy) (λ 426 nm, ϵ 300 M^{-1} cm^{-1}),[27] and Tp$^{i\mathrm{Pr}}$MoOS(OAr) (λ 503−540 nm, ϵ ca. 900 M^{-1} cm^{-1}).[30] The bands are assigned to S → Mo ligand-to-metal charge-transfer transitions. In contrast, oxomolybdenum(IV) complexes such as Tp*MoO(S_2PR_2)[32] and Tp*MoO(pyS_2)[31] are green and exhibit d−d bands at ca. 680 nm (ϵ ca. 100 M^{-1} cm^{-1}).

Crystal Structures. The crystal structure of Tp*MoOS($S_2PPr^i_2$) has been communicated;[28] full details of this structure, along with that of Tp*MoOS(S_2PPh_2) (Figure 1), are presented here. Selected bond distances and angles are given in Table 2. The six-coordinate, distorted-octahedral molecules feature a tridentate *fac*-Tp* ligand, a terminal oxo ligand, and a novel fragment formed by weakly associated sulfido and monodentate $S_2PR_2^-$ ligands. The overall structures of both molecules are very similar, but the metal−ligand distances are marginally shorter (by ca. 2%) in Tp*MoOS(S_2PPh_2). The structure of Tp*MoOS($S_2PPr^i_2$) is characterized by Mo−O1, Mo−S1, and Mo−S2 distances of 1.702(4), 2.227(2), and 2.431(2) Å, respectively. The corresponding distances in Tp*MoOS(S_2PPh_2) are 1.662(3), 2.200(2), and 2.389(2) Å. The Mo═S distances are comparable to values reported for MoOSCl_2($OPPh_3$)$_2$ [2.249(7) Å[50]] and MoOS($OSiPh_3$)$_2$(phen) [2.257(2) Å[27]]. A shorter Mo═S distance of 2.132(2) Å has been reported for Tp$^{i\mathrm{Pr}}$MoOS($OC_6H_4{}^s$Bu-2).[30] The Mo═S distances are marginally longer than those determined by EXAFS for the terminal sulfido ligand in various molybdenum hydroxylases.[16] For both molecules, the P1−S2 distances are ca. 0.05 Å longer than the P1−S3 distances. The S1···S3 distances of 2.396(3) Å for Tp*MoOS($S_2PPr^i_2$) and 2.383(2) Å for Tp*MoOS(S_2PPh_2) are both considerably longer than those characteristic of S−S single bonds (typically 2.05 Å[51]). The Mo−N distances range from 2.388(5) to 2.194(4) Å, and the ordering of Mo−N bond lengths (Mo−N11 > Mo−N31 > Mo−N21) follows the expected trans influences of the ligands, viz., Mo═O > Mo═S > Mo−SP. The Mo atoms are displaced toward the oxo group and out of the equatorial planes defined by the S1, S2, N21, and N31 atoms; the displacements were 0.226 and 0.231 Å for the isopropyl and phenyl derivatives, respectively. This distortion is associated with obtuse O1−Mo−S1 and O1−Mo−S2 angles. The Mo−O1 and Mo−N11 bonds are inclined away from the imaginary line through Mo and perpendicular to the equatorial plane; this is reflected in O1−Mo−N11 angles of 161.8(2)° and 163.5(2)° for Tp*MoOS($S_2PPr^i_2$) and Tp*MoOS(S_2PPh_2), respectively. Steric interactions between the dithiophosphinate R groups

(50) Romanenko, G. V.; Podberezskaya, N. V.; Fedin, V. P.; Geras'ko, O. A.; Fedorov, V. E.; Bakakin, V. V. *Z. Stuck. Khim. (Trans.)* **1988**, *29*, 79.
(51) Orpen, A. G.; Brammer, L.; Allen, F. H.; Kennard, O.; Watson, D. G.; Taylor, R. *J. Chem. Soc., Dalton Trans.* **1989**, S1.

and the C11 methyl group of Tp* result in a canting of the P atom out of the equatorial plane toward the oxo ligand.

The structural parameters are consistent with an oxosulfidomolybdenum(VI) formulation. The short Mo−S1 distances are indicative of a strong π interaction between these atoms, while the long S1···S3 distances confirm only a weak interaction between these S atoms. Terminal sulfidomolybdenum and alkane thiolate Mo−S bonds are characterized by median Mo−S distances of 2.133 and 2.408 Å, respectively.[51] The lengthening of the Mo−S1 bond is to be expected upon interaction of S1 with another S atom (vide infra). No previous structures containing the (S)MSP(S) moiety are available for comparison, but the S1···S3 distances are significantly longer than S−S single bonds in dithio complexes (2.0−2.10 Å),[51−53] polysulfido complexes,[52,54] and elemental S.[55] However, the S1···S3 distances are comparable to the partial[56] and easily cleaved[57] S−S partial bond in the dithionite ion $[O_2SSO_2]^{2-}$ and a number of complexes containing S···SO_x interactions[58] and electronically unusual organic compounds such as 1,6,6aλ^4-trithiapentalene.[59] A bond order of $^1/_3$ may be calculated empirically for the S1···S3 bonds. Assuming double and single S−S bond distances of 1.89 Å (for gaseous S_2) and 2.05 Å, respectively, and using the derived equation $D(n) = D(1) - 0.66 \log n$, where $D(n)$ and $D(1)$ are the bond distances for bonds of order n and 1, respectively, an estimated bond order of $^1/_3$ may be obtained for the partial S···S bond in the complexes.[60] Similarly, a bond order of ca. 2 may be derived for the Mo−S1 bond of both complexes. In the structurally characterized W analogue, Tp*$WOS(S_2PPh_2)$, the uncoordinated thiophosphinate S atom is also proximal to the terminal sulfido ligand, but the W═S [2.162(3) Å] and S···S [3.266(4) Å] distances are quite different from those of the title complexes and indicative of a negligible degree of S−S bonding.[61] The possible bonding interactions in the complexes have been previously discussed.[28]

XAS. Mo and S K-edge XAS spectra were recorded for Tp*$MoOS(S_2PR_2)$ and the dioxo analogues, Tp*$MoO_2(S_2PR_2)$.[32] The positions of the Mo K-edges of the oxosulfido complexes are 3.4 eV lower in energy than those of the corresponding dioxo complexes, consistent with a small reduction of the effective nuclear charge of Mo as a result of (i) sulfido ligation and/or (ii) partial reduction of the metal center as a consequence of the S···S interaction. A difference in Mo K-edge energies of 2 eV has been reported for $MoOE(OSiPh_3)_2L$ (E = O, S), where an S···S interaction is absent.[27] Edge features characteristic of terminal oxo ligation are present in all spectra, with those of Tp*$MoO_2(S_2PR_2)$ being more pronounced because of the greater number of oxo groups and enhancement of the 1s → 4d transition through greater p-orbital mixing. The results of the EXAFS analyses for the complexes are summarized in Table 3. The overall best fits were obtained with one oxo ligand at 1.69 Å, a sulfido ligand at 2.25 Å, a thiolate ligand at 2.44 Å, and three N donor atoms at 2.29 Å. Similar results were obtained in solution, indicating that the solid-state structure is maintained upon dissolution (vide infra). It is likely that the Mo═S distances are overestimated because of partial cancellation with the Mo−N EXAFS. The EXAFS results are consistent with the X-ray crystal structures determined for the complexes.

Table 3. EXAFS Curve-Fitting Results[a]

compound	N Mo−X	R (Å)	σ^2 (Å^2)	E_0 (eV)
Tp*$MoOS(S_2PPr^i_2)$	1 Mo═O	1.693(3)	0.0013(2)	−9.80
	1 Mo═S	2.245(8)	0.0024(5)	
	1 Mo−S	2.442(4)	0.0021(5)	
	3 Mo−N	2.29(1)	0.0056(2)	
Tp*$MoOS(S_2PPh_2)$	1 Mo═O	1.680(2)	0.0023(1)	−15.69
	1 Mo═S	2.256(6)	0.0032(8)	
	1 Mo−S	2.417(4)	0.0043(1)	
	3 Mo−N	2.29(1)	0.0055(6)	

[a] Coordination number N, interatomic distance R (Å), and (thermal and static) mean-square deviation in R (the Debye−Waller factor) σ^2 (Å^2). The values in parentheses are estimated standard deviations (precisions) obtained from the diagonal elements of the covariance matrix. We note that the accuracies will be somewhat larger than the precisions, typically ±0.02 Å for R and ±20% for N and σ^2.

The similarity of the solution and solid-state S K-edge XAS spectra of each complex (Figure 2) indicates that the S···S intramolecular interaction is maintained upon dissolution, with the S K-edge being a distinctive indicator of the molecular structure.[62] Each spectrum displays peaks at ca. 2468, 2470, and 2472 eV. The feature at 2468 eV in Tp*$MoOS(S_2PPh_2)$ is considerably sharper and more intense than the corresponding feature in the spectrum of Tp*$MoOS(S_2PPr^i_2)$. This may result from the polymorphism and crystallographic disorder present in the latter but not the former. The low-energy band (ca. 2467.8 eV) in the spectra of Tp*$MoOS(S_2PR_2)$ is attributed to a S 1s → σ* transition associated with the disulfido moiety. This band occurs at a higher energy than the S 1s → π* transition in Tp^{iPr}MoOS(OAr) complexes containing an unperturbed oxosulfidomolybdenum(VI) moiety (ca. 2466 eV).[30] A dative Mo═S···S

(52) Pilato, R. S.; Eriksen, K. A.; Greaney, M. A.; Stiefel, E. I.; Goswami, S.; Kilpatrick, L.; Spiro, T. G.; Taylor, E. C.; Rheingold, A. L. *J. Am. Chem. Soc.* **1991**, *113*, 9372.

(53) Other examples of mononuclear M−S−S− complexes include the following. (a) $MoO(S_2CPh)(S_3CPh)$: Tatsumisago, M.; Matsubayashi, G.; Tanaka, T.; Nishigaki, S.; Nakatsu, K. *J. Chem. Soc., Dalton Trans.* **1982**, 121. (b) $CpW(CO)_3(S_xR)$: Shaver, A.; Hartgerink, J.; Lai, R. D.; Bird, P.; Ansari, N. *Organometallics* **1983**, *2*, 938. (c) $Cp_2Ti\{S_2C_2(CO_2Me)_2\}$: Giolando, D. M.; Rauchfuss, T. B.; Rheingold, A. L.; Wilson, S. R. *Organometallics* **1987**, *6*, 667. (d) $Cp_2Ti(S_7NR)$: Bergemann, K.; Kustos, M.; Krüger, P.; Steudel, R. *Angew. Chem., Int. Ed. Engl.* **1995**, *34*, 1330.

(54) Draganjac, M.; Rauchfuss, T. B. *Angew. Chem., Int. Ed. Engl.* **1985**, *24*, 742.

(55) Steudel, R. *Angew. Chem., Int. Ed. Engl.* **1975**, *14*, 655.

(56) (a) Harcourt, R. D. *J. Mol. Struct. (Theochem.)* **1989**, *186*, 131. (b) Kiers, C. Th.; Vos, A. *Acta Crystallogr., Sect. B* **1978**, *34*, 1499.

(57) Lynn, S.; Rinker, R. G.; Corcoran, W. H. *J. Phys. Chem.* **1964**, *68*, 2363.

(58) Examples include: (a) Kubas, G. J.; Wasserman, H. J.; Ryan, R. R. *Organometallics* **1985**, *4*, 2012. (b) Kubas, G. J.; Ryan, R. R.; Kubat-Martin, K. A. *J. Am. Chem. Soc.* **1989**, *111*, 7823. (c) Darensbourg, M. Y.; Tuntulani, T.; Reibenspies, J. H. *Inorg. Chem.* **1995**, *34*, 6287.

(59) (a) Cimiraglia, R.; Hofmann, H.-J. *J. Am. Chem. Soc.* **1991**, *113*, 6449 and references cited therein. (b) Brown, A. S.; Smith, V. H., Jr. *J. Chem. Phys.* **1993**, *99*, 1837.

(60) Pauling, L. *The Nature of the Chemical Bond*, 3rd ed.; Cornell University Press: Ithaca, NY, 1960; p 239.

(61) Thomas, S.; Eagle, A. A.; Sproules, S. A.; Hill, J. P.; White, J. M.; Tiekink, E. R. T.; George, G. N.; Young, C. G. *Inorg. Chem.* **2003**, *42*, 5909.

(62) Pickering, I. J.; Prince, R. C.; Divers, T.; George, G. N. *FEBS Lett.* **1998**, *441*, 11.

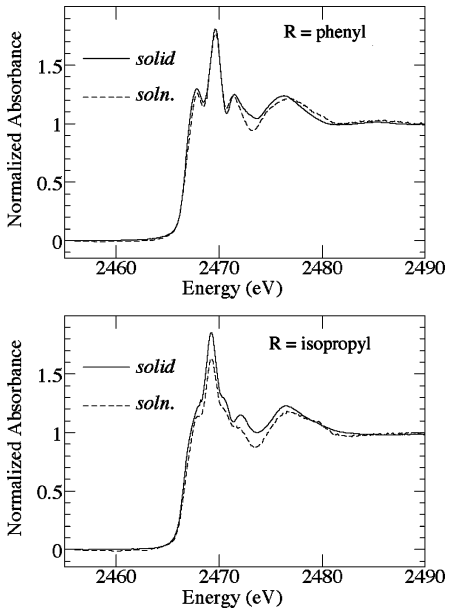

Figure 2. Solution and solid-state S K-edge XAS spectra of the phenyl (top) and isopropyl (bottom) derivatives of Tp*MoOS(S_2PR_2).

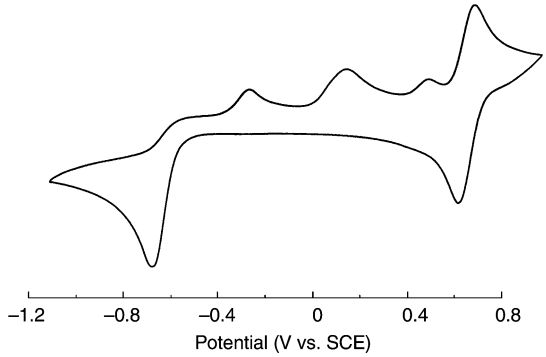

Figure 3. Cyclic voltammogram of Tp*MoOS($S_2PPr^i_2$) in MeCN (scan three) showing the reversible oxidation at +0.66 V, the irreversible reduction at ca. −0.6 V, and the associated oxidation processes.

interaction of the type previously mooted[28] (vide infra) would be expected to raise the energy of the lowest unoccupied molecular orbital (LUMO), which would be expected to exhibit a degree of Mo═S π^* character, as well as S···S σ^* character. An equivalent band is absent from the spectrum of Tp*MoO_2(SPh), consistent with the absence of the terminal sulfido ligand. The strong band at ca. 2469 eV in the spectra of the title complexes is also present in the spectra of $NH_4S_2PR_2$, Tp*$MoO_2(S_2PPh_2)$, and Tp*WOS(S_2PPh_2); this band is clearly associated with transitions from the 1s orbital on the thiophosphinate S atoms.

Electrochemistry and Reactivity. (a) Cyclic Voltammetry. The isopropyl and phenyl derivatives were the focus of electrochemical and reactivity studies described in Scheme 1 and the sections to follow. The cyclic voltammograms of the complexes (see Figure 3) exhibited an electrochemically reversible oxidation at +0.66 V, characterized by ΔE_{pp} and I_{pa}/I_{pc} values close to those observed for the reversible $[FeCp_2]^+/FeCp_2$ couple under the same conditions and indicative of a one-electron oxidation producing the cation $[Tp^*MoO(S_3PR_2)]^+$. This was the only process observed in scans from 0 to +0.8 V. When the scans were extended, an irreversible cathodic wave at ca. −0.80 V was observed, with this process being requisite for the appearance of three oxidative processes between −0.4 and +0.5 V.

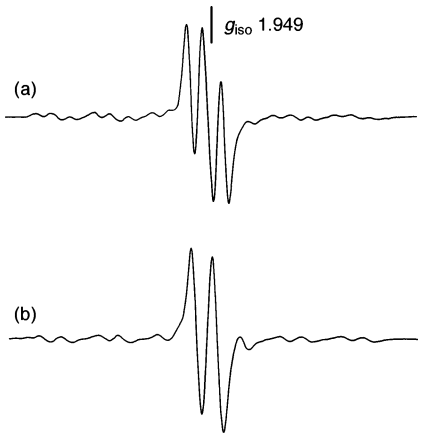

Figure 4. (a) Room-temperature solution EPR spectrum of Tp*Mo^VO-(OH)($S_2PPr^i_2$) generated in the reaction of Tp*MoOS($S_2PPr^i_2$) with 0.5 equiv of cyanide in wet solvents. (b) Room-temperature solution EPR spectrum of Tp*Mo^VO(OD)($S_2PPr^i_2$) generated as above in the presence of D_2O.

(b) Reactions with Cyanide. The reaction of Tp*MoOS-(S_2PR_2) with >1 mol equiv of cyanide under anaerobic conditions resulted in the quantitative formation of Tp*MoO-(S_2PR_2) and 1 equiv of thiocyanate, which was detected colorometrically using Sörbo's reagent.[63] Under aerobic conditions, subsequent conversion of Tp*MoO(S_2PR_2) to Tp*MoO_2(S_2PR_2) was observed. EPR-active (hydroxo)-oxomolybdenum(V) species, Tp*$Mo^VO(OH)(S_2PR_2)$, were generated in the reactions of Tp*MoOS(S_2PR_2) with 0.5 equiv of cyanide in wet solvents. These complexes were characterized by triplet EPR signals with $g \sim 1.950$, $a(^1H) = 12 \times 10^{-4}$ cm^{-1}, and $a(^{31}P) = 12 \times 10^{-4}$ cm^{-1} (Figure 4a).[32] When the reactions were performed in the presence of D_2O, the deuterated species, Tp*$Mo^VO(OD)(S_2PR_2)$, with doublet EPR signals, were generated (Figure 4b). Under anaerobic conditions, the (hydroxo)oxomolybdenum(V) species were stable for several hours but EPR activity eventually diminished. Introduction of O_2 led to an instantaneous loss of EPR activity.

(c) Reactions with Triphenylphosphine. ^{31}P NMR and associated studies revealed that the reaction of Tp*MoOS-(S_2PR_2) and >1 mol equiv of PPh_3 produced Tp*MoO(S_2-PR_2) and 1 equiv of $SPPh_3$. When less than 1 equiv of PPh_3 was employed in the reactions, stoichiometric quantities of Tp*MoO(S_2PR_2) and $SPPh_3$, as well as unreacted Tp*MoOS-(S_2PR_2), were the only detectable solution species. These reactions were not affected by the presence of water in the system.

(d) Generation of Mo(V) Complexes. EPR-active Mo-(V) species were generated upon chemical reduction *and* oxidation of the Tp*MoOS(S_2PR_2) complexes. Only a single Mo(V) species was detected in each case, but the extent of the reaction and the level of the Mo(V) species produced were not quantified. Ferrocenium-induced oxidations are expected to be incomplete in accord with electrochemical data (vide infra).

(63) Sörbo, B. *Biochim. Biophys. Acta* **1957**, *24*, 324.

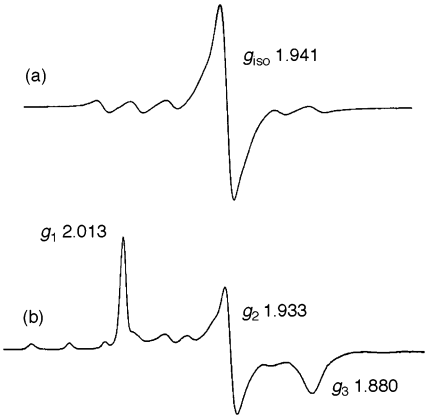

Figure 5. (a) Room-temperature solution EPR spectrum of $[Tp^*Mo^{V}OS(S_2PPr^i_2)]^-$ generated upon reaction of $Tp^*MoOS(S_2PPr^i_2)$ with excess NBu^n_4SH in THF/CH_3CN (9:1). (b) Frozen-glass EPR spectrum of $[Tp^*Mo^{V}OS(S_2PPr^i_2)]^-$ generated as above.

Table 4. EPR Parameters for Mo(V) Complexes[a]

compd	g_{iso}	g_1	g_2	g_3	$a(^1H/^{31}P)$	$a(^{95,97}Mo)$
$Tp^*MoO(OH)(S_2PPr^i_2)$	1.950				12.3	45.3
$Tp^*MoO(OH)(S_2PPh_2)$	1.949				12.0	45.8
$[Tp^*MoOS(S_2PPr^i_2)]^-$	1.938					43.5
$[Tp^*MoOS(S_2PPh_2)]^-$	1.934					43.5
$[Tp^*MoOS(S_2PPr^i_2)]^-$	1.941	2.013	1.933	1.880		A_1 43.4
$[Tp^*MoOS(S_2PPh_2)]^-$	1.939	2.012	1.932	1.877		A_1 43.5
$[Tp^*MoO(S_3PPr^i_2)]^+$	1.949	1.993	1.938	1.916	24.2	44.7
$[Tp^*MoO(S_3PPh_2)]^+$	1.947	1.991	1.936	1.912	24.2	44.5
XnO very rapid	1.976	2.025	1.955	1.949		

[a] Conditions and solvents are described in the text. Isotropic data were obtained from solution spectra at room temperature; anisotropic data were obtained from frozen-glass samples at 77 K. Units of a, 10^{-4} cm^{-1}.

(e) Upon Reduction. The unstable oxosulfidomolybdenum(V) anion formed upon reduction [cf. cyclic voltammetry (vide supra)] can be stabilized under specific chemical conditions. The reaction of $Tp^*MoOS(S_2PR_2)$ with excess NBu^n_4SH in THF/CH_3CN (9:1) at ambient temperature resulted in an immediate color change from red to brown, and frozen-glass samples, prepared within 5 s of mixing the reagents, exhibited EPR signals characteristic of oxosulfidomolybdenum(V) species, viz., $[Tp^*Mo^{V}OS(S_2PR_2)]^-$ (Figure 5). The frozen-glass spectra were highly anisotropic (Table 4), with $g_1 > g_e = 2.0023$, while room-temperature solution spectra (obtained upon thawing the initial sample) exhibited characteristically broad signals. No ^{31}P superhyperfine coupling was observed in any spectrum, consistent with the severing of the S···S interaction upon formal one-electron reduction of Mo(VI) and the formation of an oxosulfidomolybdenum(V) species. The same EPR signals were generated upon reduction using cobaltocene. Moreover, the EPR spectra were identical with those generated upon anaerobic incubation of $Tp^*MoO_2(S_2PR_2)$ complexes with excess NBu^n_4SH; these signals are ascribed to $[Tp^*Mo^{V}OS(S_2PR_2)]^-$ complexes, formed upon sulfidation of the initial reduction product, $[Tp^*Mo^{V}O_2(S_2PR_2)]^-$.[32] In situ generated $[Tp^*Mo^{V}OS(S_2PR_2)]^-$ were very stable under anaerobic conditions, and their EPR signals persisted for many days; this is ascribed to the presence of the highly basic and reducing hydrosulfido anion. Admission of O_2 resulted in an immediate loss of EPR activity, with the formation of $Tp^*MoOS(S_2PR_2)$ and $Tp^*MoO_2(S_2PR_2)$; $Tp^*MoOS(S_2PR_2)$ was formed in high yield when *dried* O_2 was employed, while the use of *undried* O_2 led to the formation of $Tp^*MoO_2(S_2PR_2)$ at the expense of $Tp^*MoOS(S_2PR_2)$. This behavior parallels the oxidation of $[Tp^*MoOS(S_2PR_2)]^-$ generated by the reaction of $Tp^*MoO_2(S_2PR_2)$ with NBu^n_4SH.[32] All attempts to protonate the $[Mo^{V}OS]^+$ complexes, even with carefully dried CF_3COOH, resulted in an immediate loss of the EPR signals.

Figure 6. Room-temperature EPR spectrum of $[Tp^*MoO(S_3PPr^i_2)]^+$ prepared by the reaction of $Tp^*MoOS(S_2PPr^i_2)$ with excess $[FeCp_2]PF_6$ in THF/CH_3CN (9:1).

(f) Upon Oxidation. Chemical oxidation of the complexes by $[FeCp_2]PF_6$ resulted in the formation of a single EPR-active species, assigned as the Mo(V) cation, $[Tp^*MoO(S_3PR_2)]^+$. Thus, although the reduction potentials of $Tp^*MoOS(S_2PR_2)$ [ca. +0.2 V vs $[FeCp_2]^+/FeCp_2$ in THF/CH_3CN (9:1)] disfavor oxidation, an equilibrium concentration of $[Tp^*MoO(S_3PR_2)]^+$ was readily detectable by EPR spectroscopy under the conditions used [10 mM $Tp^*MoOS(S_2PR_2)$, >10-fold excess of $[FeCp_2]PF_6$]. The $[Tp^*MoO(S_3PR_2)]^+$ cations exhibited a doublet EPR signal at $g \sim 1.949$ with $a(^{31}P) = 24.2 \times 10^{-4}$ cm^{-1} (Figure 6). A rhombic frozen-glass spectrum with unresolved coupling features was observed (Table 4). The signal was stable over a period of days at room temperature, but other features were observed to grow in with time. The addition of water to the reaction mixture did not influence the products formed (as monitored by EPR).

The oxidation of the complexes provides an interesting example of internal redox. The process is electrochemically reversible and results in the generation of a cationic species proposed to contain a perthiophosphinate ligand with an S−S single bond (inferred from EPR spectroscopy). The signals of the cations have a higher g_{iso} value and are much less anisotropic than those of the anions above, and the observation of ^{31}P superhyperfine coupling is consistent with the tethering of the P atom in a position permitting electronic communication with the d_{xy} magnetic orbital. We propose that the overall one-electron oxidation comprises the formal coupling of a one-electron metal reduction and a two-electron oxidation of the nascent disulfide bond between S1 and S3, as shown explicitly in eqs 8−10. This behavior is complemented by direct oxidation and induced internal redox (reduction) reactions involving $Tp^*Mo^{IV}O(pyS_2)$, which produce $[Tp^*Mo^{V}O(pyS_2)]^+$ and $[Tp^*Mo^{V}OS(pyS)]^-$, respectively.[31] Related behavior is also observed for analogous W complexes.[61]

$$Mo^{VI} + e^- \rightarrow Mo^{V} \quad (8)$$

$$Mo^{VI}{=}S{\cdots}S{=}P \rightarrow [Mo^{VI}{-}S{-}S{-}P]^{2+} + 2e^- \quad (9)$$

$$\text{Net:} \quad Mo^{VI}{=}S{\cdots}S{=}P \rightarrow Mo^{V}{-}S{-}S{-}P^+ + e^- \quad (10)$$

(g) Biomimetic Behavior. The combined cyanolysis and sulfidation/oxidation reactions described above and summarized in Scheme 1 provide the closest model available for the cyanolysis/reactivation reactions of the molybdenum hydroxylases. Thiocyanate and an oxomolybdenum(IV) complex are initially formed; in dry solvents, excess cyanide rapidly reacts to form Tp*MoO(S_2PR_2), containing a bidentate dithiophosphinate ligand, which is only slowly converted to Tp*MoO_2(S_2PR_2) in the presence of oxygen and water. In the presence of water, 0.5 equiv of cyanide produces Tp*MoO(OH)(S_2PR_2) via comproportionation and hydrolysis reactions. The (hydroxo)oxomolybdenum(V) species models the "slow" center observed during cyanide deactivation of xanthine oxidase in the presence of physiological oxidants. In the reaction of Tp*MoOS(S_2PR_2) with PPh_3, the generation of Tp*MoO(OH)(S_2PR_2) appears to be prevented by the steric bulk and hydrophobicity of the departing $SPPh_3$ molecule, permitting chelation of the dithiophosphinate ligand to be competitive with aquation and coupled-electron−proton-transfer chemistry. The reactions with cyanide and PPh_3 are interpreted in terms of nucleophilic attack at the sulfido S atom (on the π^* Mo═S LUMO). The reaction of Tp*MoO_2(S_2PR_2) with sulfide results in the sequential generation of [Tp*MoO_2(S_2PR_2)]$^-$ and then [Tp*MoOS(S_2PR_2)]$^-$. Oxidation of the latter complex with O_2 results in the regeneration of Tp*MoOS(S_2PR_2), providing a complete model for the enzyme cyanolysis/reactivation reactions.

Summary

This paper describes the synthesis and characterization of *cis*-oxosulfidomolybdenum(VI) complexes, Tp*MoOS(S_2PR_2) (R = Et, Pr^i, Ph), generated by SAT to oxomolybdenum(IV) precursors. In these six-coordinate complexes, the sulfidomolybdenum moiety is stabilized by an intramolecular S···S interaction involving the monodentate dithiophosphinate ligand. This weak interaction only slightly perturbs (lengthens) the Mo═S bond, which falls close to the range typical of sulfidomolybdenum complexes. The presence of the S···S interaction does not mask the intrinsic chemistry (atom transfer, etc.) of the sulfido ligand. The redox reactions documented underscore the remarkable redox interplay of Mo and S, a facet of their chemistry likely to be important in enzyme behavior.

Acknowledgment. We thank Drs. Michelle K. Taylor and Hugh H. Harris for experimental assistance and helpful discussions and gratefully acknowledge the financial support of the Australian Nuclear Science and Technology Organization (for travel to SSRL) and the Australian Research Council. SSRL is funded by the Department of Energy (DOE) BES with further support by DOE OBER and the National Institutes of Health.

Supporting Information Available: Crystallographic data in CIF format. This material is available free of charge via the Internet at http://pubs.acs.org.

IC061213D